Journal of Hydroscience and Hydraulic Engineering
Vol. 22, No.2 November, 2004, 79-91

NUMERICAL STUDY OF TWO-DIMENSIONAL DENSITY SURGES

By

Juichiro Akiyama, Mirei Shige-eda
Department of Civil Engineering, Kyushu Institute of Technology
Sensuicho 1-1, Tobata, Kitakyushu 804-8550, JAPAN

Masayuki Nonaka
City of Kitakyushu, Construction Bureau
Jyounai 1-1, Kokura-Kita, Kitakyushu 803-8501, JAPAN

and

Tsutomu Yamasaki

Ministry of Land, Infrastructure and Transport,
Kyushu Regional Development Bureau
Yadomachi 316-1, Nagasaki 851-0121, JAPAN

SYNOPSIS

A numerical model based on the Simplified Marker and Cell (SMAC) method and Monotone Upstream-centered Schemes for Conservation Laws (MUSCL) technique is constructed to simulate two-dimensional density surges, initiated by a finite volume release of dense fluid into a finite ambient water depth on a horizontal bed. The density differences are due to either salinity or mixture of nearly uniform sized particles and water. The simulated results are compared with such flow characteristics as the maximum height, propagation speed, mean effective gravity force and densimetric Froude number at the front of the surges.

INTRODUCTION

In many problems of environmental concern, there are a number of practical situations in which denser fluid spreads out as a gravity current. Typical examples of such phenomena are sea-breeze fronts, the accidental release of dense industrial gases, powder-snow avalanches, turbidity currents and lock exchange flows (Simpson (22) and Hopfinger (12)).

Gravity currents can be in the form of either a starting plume or a thermal, depending on whether the source is maintained or instantaneous. A starting plume consists of a head with complex three-dimensional flow structure at the leading edge, followed by a thinner flow. The leading edge of the flow is commonly referred to as the front, which is a zone of breaking waves and intense mixing, and plays an important part in the behavior of currents. The rest is called the body, which plays an important role in the development of the flow by feeding buoyancy into the front. Consequently, the total buoyancy of the front increases along its path (Britter & Linden (9), Akiyama et al. (3)).

The instantaneously released thermal by contrast consists only of a front flow structure without a distinct body. A great deal of research has been devoted to the

Table1 Major flow characteristics of the front of conservative gravity currents

	U	H	B	Fr
Inclined plume	$\sim$ constant	$\sim x_f$	$\sim x_f^{-1}$	$\sim$ constant
Inclined thermal	$\sim x_f^{-1/2}$	$\sim x_f$	$\sim x_f^{-2}$	$\sim$ constant

determination and/or prediction of flow characteristics of inclined thermals. Hopfinger & Tochon-Danguy (13) analyzed powder-snow avalanches as two-dimensional inclined thermals with snow entrained from the powder-snow cover ahead of the avalanches. Beghin et al. (6) investigated theoretically and experimentally the motion of conservative two-dimensional inclined thermals on slope angles ranging mainly from 5° to 90°. Their experimental study shows that the length-to-height ratio, spatial growth rate and entrainment coefficient are all functions of the bottom slope angle. In addition, a thermal theory, which is basically an extension of the free vertical thermal model by Morton et al. (18), has been proposed by Beghin et al. (6). Akiyama & Ura (2) have conducted an extensive experimental as well as theoretical study of inclined thermals with small density differences on slope angles ranging from 5° to 90°, aiming to provide more complete information than Beghin et al. (6). It was found that both the spatial growth rates of the maximum height and the entrainment coefficients obtained in the study were of substantially larger magnitude than those of Beghin et al. (6). In the analysis, a thermal model was developed that included a resistance term, previously ignored by Beghin et al.(6).

In summary, the major flow characteristics of front of conservative gravity currents on inclines are tabulated in Table 1, where U = propagation speed, H = maximum height; B = mean effective gravity force ($=\epsilon$ g); Fr =densimetric Froude number ($U/\sqrt{\epsilon g H}$); ϵ = relative density difference; g = acceleration due to gravity; x_f = traveling distance measured from the origin to the foremost part of the front.

Akiyama et al. (1) extended the range of investigation of Akiyama & Ura (2) to low slope angles ranging from 1° to 5°. It was found that, in the range, the total initial effective gravity force W_0 within the thermal body was not conserved along its path. The effective gravity force W within the thermal body was found to be less than 50% of W_0, and larger amount of total buoyancy force remains within the thermal body with larger slope angle. The study also indicates that when a slope angle is less than 3°, the motion of the flow changes from that could be described by the thermal theory.

A number of studies have been conducted on the motion of a two-dimensional thermal or a density surge on a horizontal channel. Huppert & Simpson (16) showed that an almost constant velocity regime is expected in the early stages of a finite volume release. They called this as the "slumping regime". In this regime the front height H and the densimetric Froude number Fr are approximately constant with x_f. The value of Fr in the slumping regime has been estimated experimentally by several investigators. For instance, Hoult (15) proposed Fr=1.18. However, evolution of such flow characteristics as the front propagation speed and the maximum front height with time, or along its path remains uncertain, perhaps due to difficulties in estimating loss of W_0 from the front of a density surge.

The motion of the fluid surrounding the gravity currents also depends on the fractional depth of the current H/h, where h is the depth of the surrounding fluid. The slumping regime comes to an end when the fractional depth falls to about one tenth. In the inertia-buoyancy regime, where the inertia and buoyant force are balanced, the front speed U will decrease as $t^{-1/3}$, where t=time. Huppert & Simpson (16) proposed the following empirical

relationships for the front Froude number Fr of gravity currents on a horizontal channel, based on the results from steady-state experiments reported by Simpson & Britter (23) as well as from additional data obtained by Huppert & Simpson (16).

$$F_r = \begin{cases} 1.19 & \text{for } H/h \leq 0.075 \\ 0.5(H/h)^{-1/3} & \text{for } H/h = 0.075 \sim 1 \end{cases} \tag{1}$$

Various theories which account for the front of a density surge resulting from instantaneous release have been proposed. Hoult (15) and Huppert & Simpson (16) used an order of magnitude evaluation of forces in the governing equations. Benjamin (7) and Yih (25) used simple energy considerations, Rottman & Simpson (20), Bonnecaze et al.(8), Jha et al. (17) solved the depth-averaged shallow-water equations as the initial-value problem, imposing the front condition. However, an order of magnitude evaluation requires extensive experimental work in order to determine proportional constants. Energy considerations require an appropriate estimation of energy loss in the front, however, this is actually impossible. By solving shallow-water equations, the front propagation speed can be predicted if an appropriate front condition is imposed, however, the shape of the front cannot be reproduced, because of the nature of the method.

Theoretical analyses are helpful in understanding the fundamentals of the motion of gravity currents, including the density surge. However, gravity currents in practice take place under the complicated conditions, such as the limitation of ambient water depth, the presence of density gradient and others. This necessitates the development of a numerical model. A number of numerical studies for various types of gravity currents have been performed ((10), (19), (14), (26), (4), (11)). Among these studies, Eto & Fukushima (11) examined conservative density surges on the inclined surface. Hosoda et al. (14) and Nakayama & Satoh (19) dealt with conservative gravity currents on the horizontal surface. The former was mainly concerned with the mixing process of a lock exchange flow, and the latter with a plume geometry of the front and the turbulent heat flux on the interface. To the best our knowledge, there exists no numerical model, that is able to adequately simulate the motion of density surges on horizontal surface.

In this study, a numerical model, based on the Simplified Marker and Cell(SMAC) method and Monotone Upstream-centered Schemes for Conservation Laws (MUSCL) technique, was constructed in order to simulate two-dimensional saline as well as suspension density surges on a horizontal bed, produced by a finite volume release of dense fluid into a finite ambient water depth. The simulated results were verified by means of experimental results of maximum height, propagation speed, buoyancy and densimetric Froude number of the front of the surges. Comparison between the simulated results and the empirical relationship, proposed by Huppert & Simpson (16), was also presented. The effects of the fractional depth on the motion of the current were examined by means of numerical experiments. In addition, the flow characteristics in the slumping regime as well as the inertia-buoyancy regime were also clarified.

GOVERNING EQUATIONS

The suspension density surges considered in this study are induced by a high concentration solid-liquid mixture fluid, hence one-equation model is employed as a two-phase flow model. The effects of particles on the motion of the currents are, therefore, considered only in the conservation of mass.

Governing equations are the conservation of volume, the equation of motion with

Boussinesq approximation, and the conservation of mass.

$$\frac{\partial u}{\partial x}+\frac{\partial v}{\partial y}=0 \tag{2}$$

$$\begin{aligned}\frac{\partial u}{\partial t}+\frac{\partial uu}{\partial x}+\frac{\partial vu}{\partial y}&=-\frac{1}{\rho_0}\frac{\partial p}{\partial x}+\nu\left(\frac{\partial^2 u}{\partial x^2}+\frac{\partial^2 u}{\partial y^2}\right)\\ \frac{\partial v}{\partial t}+\frac{\partial uv}{\partial x}+\frac{\partial vv}{\partial y}&=-\frac{1}{\rho_0}\frac{\partial p}{\partial y}+\nu\left(\frac{\partial^2 v}{\partial x^2}+\frac{\partial^2 v}{\partial y^2}\right)-\epsilon g\end{aligned} \tag{3}$$

$$\frac{\partial \epsilon}{\partial t}+\frac{\partial u\epsilon}{\partial x}+\frac{\partial (v+V_s)\epsilon}{\partial y}=D_m\left(\frac{\partial^2 \epsilon}{\partial x^2}+\frac{\partial^2 \epsilon}{\partial y^2}\right) \tag{4}$$

where t=time; u, v= flow velocities along x- and y- direction, respectively; p = pressure; ϵ = relative density difference$(=(\rho-\rho_a)/\rho_a)$; ρ = density of solid-liquid mixture; ρ_a = density of ambient fluid; ν = kinematic viscosity of fluid; D_m=diffusivity $(=\nu/S_{ct})$; S_{ct} = Schmidt number; V_s = settling velocity of a particle.

NUMERICAL METHOD AND BOUNDARY CONDITIONS

SMAC(Simplified Marker And Cell) method

The governing equations are solved numerically using Simplified Marker And Cell (SMAC) method (5). Eqs.2,3,and 4 are solved in the following order:

1. Solve Eqs.3 and 4 by using 2nd-order Adams-Bashoforth time integral method with u,v,p,ϵ at t and compute u, v at intermediate level, ϵ at the next time level, respectively as shown in Eq.5.

$$\begin{aligned}\boldsymbol{U}^p&=\boldsymbol{U}^n+\Delta t\left(-\frac{1}{\rho_0}\nabla p^n+\frac{3\left(\boldsymbol{A}^n+\boldsymbol{B}^n\right)-\left(\boldsymbol{A}^{n-1}+\boldsymbol{B}^{n-1}\right)}{2}+\boldsymbol{S}^n\right)\\ \epsilon^{n+1}&=\epsilon^n+\Delta t\frac{3\left(\epsilon^n_{add}+\epsilon^n_{diff}\right)-\left(\epsilon^{n-1}_{add}+\epsilon^{n-1}_{diff}\right)}{2}\end{aligned} \tag{5}$$

where $\boldsymbol{U}=\begin{pmatrix}u\\ v\end{pmatrix}$, $\boldsymbol{A}=\begin{pmatrix}-\left(u\frac{\partial u}{\partial x}+v\frac{\partial u}{\partial y}\right)\\ -\left(u\frac{\partial v}{\partial x}+v\frac{\partial v}{\partial y}\right)\end{pmatrix}$, $\boldsymbol{B}=\begin{pmatrix}\nu\left(\frac{\partial^2 u}{\partial x^2}+\frac{\partial^2 u}{\partial y^2}\right)\\ \nu\left(\frac{\partial^2 v}{\partial x^2}+\frac{\partial^2 v}{\partial y^2}\right)\end{pmatrix}$, $\boldsymbol{S}=\begin{pmatrix}0\\ -\epsilon g\end{pmatrix}$,

$\epsilon_{add}=-\left(\frac{\partial u\epsilon}{\partial x}+\frac{\partial v\epsilon}{\partial y}\right)$, $\epsilon_{diff}=D_m\left(\frac{\partial^2 \epsilon}{\partial x^2}+\frac{\partial^2 \epsilon}{\partial y^2}\right)$, Δt=time step size, n=index for time.

2. Using the velocities at intermediate level, solve Poisson type equation Eq.6 for a scalar potential ϕ corresponding to the time change of pressure p by using the SOR method and compute u, v, and p as shown in Eq.7 and 8. Convergence criteria of Eq.6 is set to $||\phi^{m+1}-\phi^m||/||\phi^{m+1}||<1.0\times10^{-3}$ where m=iteration number, $||\phi||=(1/N\cdot\sum_{l=1}^{N}\phi_l^2)^{1/2}$, l=index for computational grid, N=total grid number.

$$\nabla^2\phi=\frac{\rho_0}{\Delta t}\nabla\cdot\boldsymbol{U}^p \tag{6}$$

$$\boldsymbol{U}^{n+1}=\boldsymbol{U}^p-\frac{\Delta t}{\rho_0}\nabla\phi \tag{7}$$

$$p^{n+1}=p^n+\phi \tag{8}$$

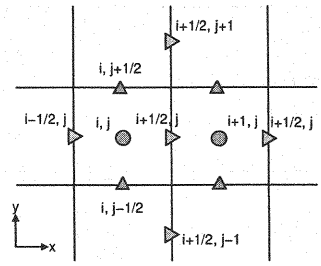

Fig.1 Staggard grids

Computational Technique for Space Derivatives

The advection terms are computed by the MUSCL method (24) to achieve stable computations. The pressure terms and viscous terms are computed by central difference. Using Staggard grids shown in Fig.1, the advection term, pressure term, and viscous term are computed respectively as follows:

Advection Terms :

$$
\begin{aligned}
&[(uf)_x]_{i+1/2,j} = \frac{-[uf]_{i,j} + [uf]_{i+1,j}}{\Delta x} \\
&[uf]_{i,j} = u_{i,j}\frac{f_{Li,j} + f_{Ri,j}}{2} - |u_{i,j}|\frac{-f_{Li,j} + f_{Ri,j}}{2} \\
&u_{i,j} = \frac{u_{i-1/2,j} + u_{i+1/2,j}}{2} \\
&[(vf)_y]_{i+1/2,j} = \frac{-[vf]_{i+1/2,j-1/2} + [vf]_{i+1/2,j+1/2}}{\Delta y} \\
&[vf]_{i+1/2,j-1/2} = \\
&v_{i+1/2,j-1/2}\frac{f_{Li+1/2,j-1/2} + f_{Ri+1/2,j-1/2}}{2} - |v_{i+1/2,j-1/2}|\frac{-f_{Li+1/2,j-1/2} + f_{Ri+1/2,j-1/2}}{2}
\end{aligned}
\tag{9}
$$

$$
v_{i+1/2,j-1/2} = \frac{v_{i/2,j-1/2} + v_{i+1,j-1/2}}{2} \tag{10}
$$

where $f_{Li,j}$, $f_{Ri,j}$, $f_{Li+1/2,j-1/2}$, $f_{Ri+1/2,j-1/2}$ = interpolated f by using MUSCL method are writen as

$$
\begin{aligned}
f_{Li,j} &= f_{i-1/2,j} + \frac{1}{4}\left[(1-\kappa)\overline{\Delta_x^-}_{i-/2,j} + (1+\kappa)\overline{\Delta_x^+}_{i-1/2,j}\right] \\
f_{Ri,j} &= f_{i+1/2,j} - \frac{1}{4}\left[(1-\kappa)\overline{\Delta_x^+}_{i+1/2,j} + (1+\kappa)\overline{\Delta_x^-}_{i+1/2,j}\right] \\
f_{Li+1/2,j-1/2} &= f_{i+1/2,j-1} + \frac{1}{4}\left[(1-\kappa)\overline{\Delta_y^-}_{i+1/2,j-1} + (1+\kappa)\overline{\Delta_y^+}_{i+1/2,j-1}\right] \\
f_{Ri+1/2,j-1/2} &= f_{i+1/2,j} - \frac{1}{4}\left[(1-\kappa)\overline{\Delta_y^+}_{i+1/2,j} + (1+\kappa)\overline{\Delta_y^-}_{i+1/2,j}\right]
\end{aligned}
\tag{11}
$$

$\overline{\Delta^+}$, $\overline{\Delta^-}$ are writen as

$$
\begin{aligned}
&\overline{\Delta_x^-}_{i-1/2,j} = \mathrm{minmod}(\Delta^+_{x\,i-1/2,j}, b\Delta^-_{x\,i-1/2,j}) \\
&\overline{\Delta_x^+}_{i-1/2,j} = \mathrm{minmod}(\Delta^-_{x\,i+1/2,j}, b\Delta^+_{x\,i+1/2,j}) \\
&\overline{\Delta_y^-}_{i+/2,j-1} = \mathrm{minmod}(\Delta^+_{y\,i+1/2,j-1}, b\Delta^-_{y\,i+1/2,j-1}) \\
&\overline{\Delta_y^+}_{i+1/2,j} = \mathrm{minmod}(\Delta^-_{y\,i+1/2,j}, b\Delta^+_{y\,i+1/2,j})
\end{aligned}
\tag{12}
$$

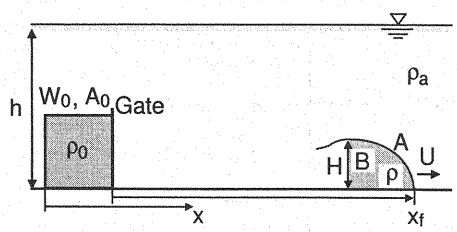

Fig.2 Sketch of a thermal on horizontal bed

Table2 Experimental conditions

Case	h	A_0 (m × m)	ϵ_0	W_0 (m^3/s^2)	d (mm)
GS	0.9	0.3 × 0.3	0.0110	0.00970	-
GP	0.5	0.2 × 0.2	0.0125	0.00490	0.044

where $\Delta^-_{x\,i-1/2,j} = f_{i-1/2,j} - f_{i-3/2,j}$, $\Delta^+_{x\,i-1/2,j} = f_{i+1/2,j} - f_{i-1/2,j}$, $\Delta^-_{y\,i+1/2,j-1} = f_{i+1/2,j-1} - f_{i+1/2,j-2}$, $\Delta^+_{y\,i+1/2,j-1} = f_{i+1/2,j} - f_{i-1/2,j-1}$, $\mathrm{minmod}(x,y) = x(|x| < |y|, x \times y > 0), y(|x| > |y|, x \times y > 0), 0(x \times y < 0)$, $b = \frac{3-\kappa}{1-\kappa}$, κ= model constant (κ=0.5 is set in this study).

Pressure Terms :

$$\left[-\frac{1}{\rho_0}\frac{\partial p}{\partial x}\right]_{i+1/2,j} = -\frac{1}{\rho_0}\frac{-p_{i,j} + p_{i+1,j}}{\Delta x} \tag{13}$$

Viscous Terms:

$$\left[\nu\left(\frac{\partial^2 u}{\partial x^2} + \frac{\partial^2 u}{\partial y^2}\right)\right]_{i+1/2,j} = \nu\left(\frac{u_{i-1/2,j} - 2u_{i+1/2,j} + u_{i+3/2,j}}{\Delta x^2} + \frac{u_{i+1/2,j-1} - 2u_{i+1/2,j} + u_{i+1/2,j+1}}{\Delta y^2}\right)$$

Continuty Equation:

$$\frac{\partial u}{\partial x} + \frac{\partial v}{\partial y} = \frac{-u_{i-1/2,j} + u_{i+1/2,j}}{\Delta x} + \frac{-v_{i,j-1/2} + u_{i,j+1/2}}{\Delta y} \tag{14}$$

where Δx, Δy = grid size in x, y direction.

Boundary Conditions

The imposed boundary conditions for u, v, ϕ, ϵ are as follows.

- side and bottom boundary:

  $u = v = 0$ (non-slip conditions), $\partial\phi/\partial n = 0$, $\partial\epsilon/\partial n = 0$

- top boundary :

  $\partial u/\partial y$=0, $v = 0$ (slip conditions), $\phi = 0$, $\partial\epsilon/\partial n = 0$, where n = direction perpendicular to boundary.

EXPERIMENTS

Experiments were conducted in a Perspex water reservoir (0.1m wide, 1.2m deep, and 7.5m long) with no bottom slope. Both conservative (Case GS) and non-conservative (Case

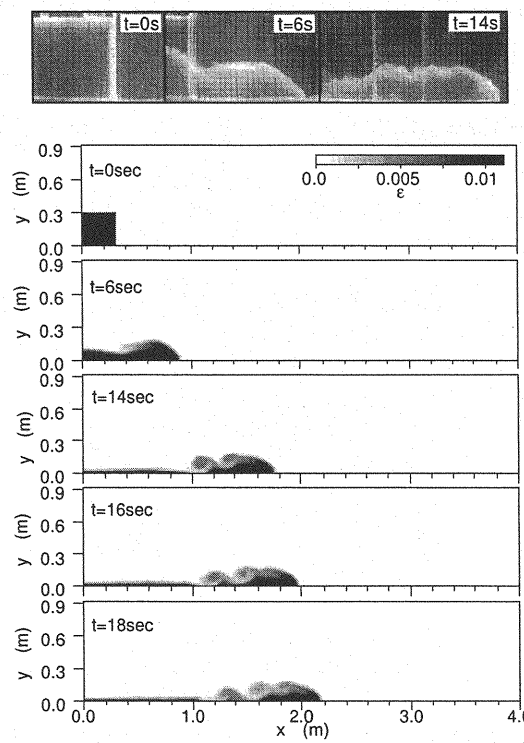

Fig.3 Photographs and computed relative density difference fields for Case GS

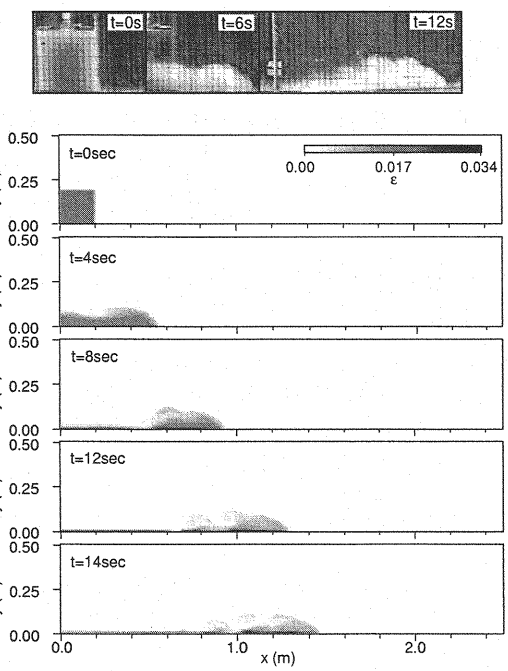

Fig.4 Photographs and computed relative density difference fields for Case GP

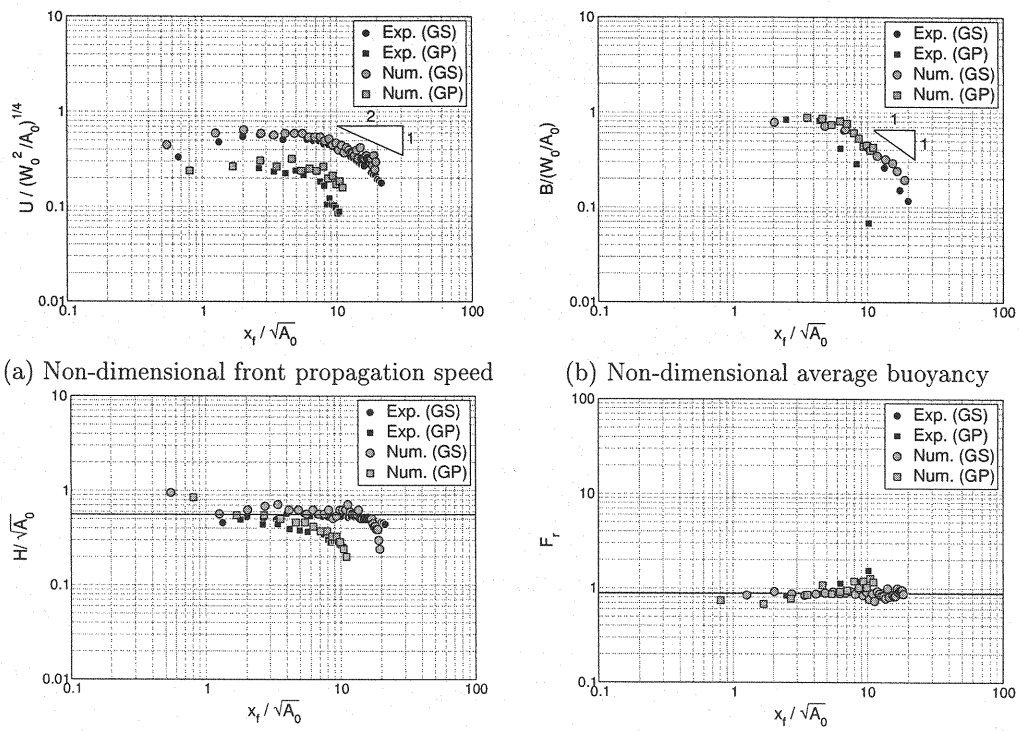

(a) Non-dimensional front propagation speed

(b) Non-dimensional average buoyancy

(c) Non-dimensional front height

(d) Densimetric Froude number F_r

Fig.5 Comparison of computed results with observed results

GP) density surges were considered. A salt-solution marked with fluorescence in Case GS or turbid water in Case GP were used to produce the flows. As shown in Fig.2, a fixed volume A_0 of dense water with density ρ_0 was instantaneously released into homogeneous fresh water body with density ρ_a, contained in the square box placed at the upstream end of the channel, by withdrawing the release gate of the box. The total initial effective gravity force W_0 is defined as $W_0 = \epsilon_0 g A_0$, where ϵ_0 =initial relative density difference $(=(\rho_0 - \rho_a)/\rho_a)$, g = accelelation of gravity. In Case GS, W_0 is defined as $csgA_0$, where c=volumetric concentration (=0~1.0), s=submerged specific gravity of a particle(=σ-1), and σ = specific gravity of a particle. Particles were glass beads with median diameter d=0.044mm and s=1.47. The particle Reynolds number $R_p(=V_s d/\nu)$ is 0.068. Experimental conditions are listed in Table 2.

The propagation speed U and shape and size(front maximum height H, front area A, front length L) of the front were quantified by a flow visualization technique; a CCD-camera was moved along with the advancement of the cloud. An analysis of the images of the clouds recorded by a digital VTR, allowed to obtain these flow characteristics, which are defined in Fig,2. The average total effective gravity force B of the front of the surges was estimated by total effective gravity force of the front W divided by A. In Case GS, W was estimated by multiplying volume by density of saline water siphoned out from the front, which was cut off from the rest of flow by inserting boards behind and front of the front. In Case GP, W was estimated by subtracting the effective gravity force of the deposited particles W_d from W_0. W_d was obtained by inserting a board behind the front and by siphoning out the deposited particles after they fully settled down on the bed.

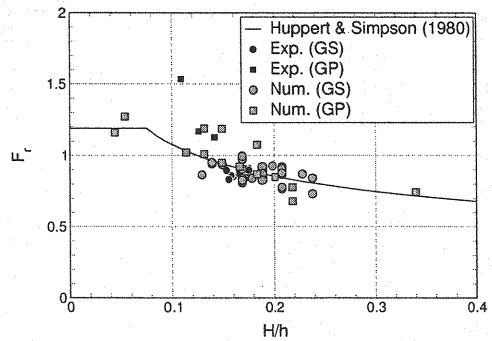

Fig.6 Densimetric Froude number F_r as function of fractional depth H/h

VERIFICATION OF THE MODEL

In the calculations performed, kinematic viscosity of fluid is set as ν=1.0×10^{-6}(m^2/s) and Schmidt number is S_{ct}=0.5. Grid size is Δx=Δy=0.02m for Case GS and Δx=0.02m, Δy=0.01m for Case GP, respectively. The falling velocity of particle V_s is computed from Rubey's equation (21). The total initial effective gravity force W_0 is well conserved throughout computation, because error in W_0 in the entire computational domain is found to be less than 1.0×10^{-6}%.

Fig.3 and 4 show experimental photographs of the surges and computed relative density difference ϵ for Case GS and Case GP, respectively. Therein the region of the computed surges is defined by $\epsilon \geq$0.0003. The forming process of the surges from static condition can be observed. Intense mixing is confined to the region just behind the front of the surges, and the mixed fluid is left behind the front.

In line with our interest in the practical aspects of modeling, the prediction of flow properties such as the propagation speed U, maximum height H, and mean effective gravity force B of the front of the surge were found to be significant.

The computed front region A is defined as ϵ=0.0003 as stated the above. It allows to determine the foremost point x_f as well as H of the front at a given time. B is estimated by dividing the total relative density difference, which was calculated from integrating relative density difference within the front, by A of the front.

Figs.5a $\sim$ 5d show the relationships between the dimensionless traveling distance $x_f/\sqrt{A_0}$ from the releasing point to the leading edge of the surge, and the dimensionless propagating speed $U/(W_0^2/A_0)^{1/4}$, the dimensionless maximum height $H/\sqrt{A_0}$, the dimensionless mean effective gravity force $B/(W_0/A_0)$, the densimetric Froude number Fr, respectively.

In Case GS, both numerical and experimental results show that $U/(W_0^2/A_0)^{1/4}$, $H/\sqrt{A_0}$, $B/(W_0/A_0)$, and Fr are almost constant with $x_f/\sqrt{A_0}$ up to the point $x_f/\sqrt{A_0} \approx$ 6. Such relationships indicate that in this particular case the slumping regime is terminated around that point.

When $x_f/\sqrt{A_0} \gtrapprox 6$, it is observed that the dependence of $U/(W_0^2/A_0)^{1/4}$ and $B/(W_0/A_0)$ on $x_f/\sqrt{A_0}$ are $U/(W_0^2/A_0)^{1/4} \sim (x_f/\sqrt{A_0})^{-1/2}$ and $B/(W_0/A_0) \sim (x_f/\sqrt{A_0})^{-1}$ respectively, while both $H/\sqrt{A_0}$ and Fr are almost constant with $(x_f/\sqrt{A_0})^{-1}$. The relationship of $U/(W_0^2/A_0)^{1/4} \sim (x_f/\sqrt{A_0})^{-1/2}$ suggests that the flow changes from the slumping regime to the inertia-buoyancy regime, because previous studies (Hoult (15), Huppert & Simpson(16), Rottman & Simpson(20)) show that such a relationship as $U \sim t^{-1/3}$ in the inertia-buoyancy regime exists. This relationship yields that $x_f \sim t^{2/3}$. It

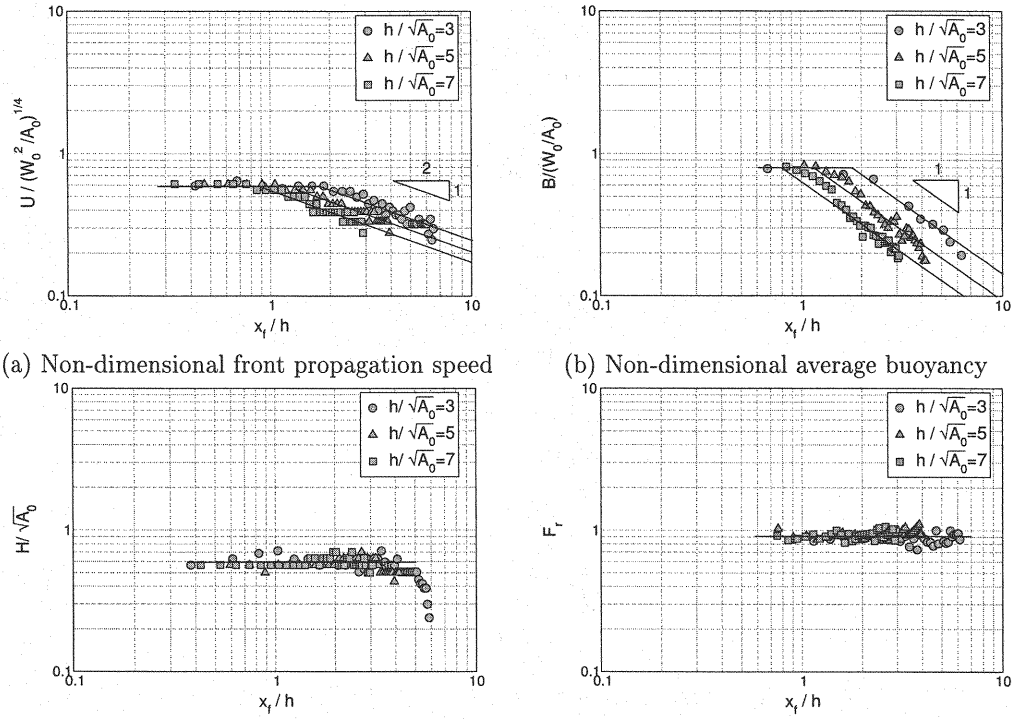

(a) Non-dimensional front propagation speed

(b) Non-dimensional average buoyancy

(c) Non-dimensional front height

(d) Densimetric Froude number F_r

Fig.7 Non-dimensional Characteristic Variables as a function of x_f/h

is apparent from these relationships that $U \sim x_f^{-1/2}$ is valid in the inertia-buoyancy regime.

Fig.6 shows a comparison between the numerical and experimental results regarding dependence of the front Froude nember Fr on the fractional depth of the current H/h. In the figure, the empirical relationships (Eq.1) proposed by Huppert & Simpson (16) are also plotted. It can be observed that calculated Fr scattered around Eq.1, and hence dependence of F_r on H/h is simulated well by the present model.

In Case GP, it may be seen from these figures that the present model is capable to appropriately simulate the behavior of suspension density surge in the slumping regime. However, the model fails to simulate the flows in the inertia-buoyancy regime. In this region, experimental results of U, B and H fall more rapidly than those of the conservative density surge. This may be due to the loss of buoyancy resulting from particle settling from the flow. It may be indicated that a SGS model, which appropriately handles small scale turbulence, and the treatment of particle deposition are required to simulate the behaviors of a suspension density surge.

Since the present model simulates well the motion of the conservative density surge, the effects of such an additional parameter that may significantly affect the motion of the surge, as the ratio $h/\sqrt{A_0}$ of the ambient water depth h to the initial height $\sqrt{A_0}$ of the surge, are examined through numerical experiments. Simulated results are presented in Fig.7. It can be observed from these figures that the transition point from the slumping regime to the inertia-buoyancy regime is controlled by the parameter $h/\sqrt{A_0}$ and the transition takes place in the shorter traveling distance when $h/\sqrt{A_0}$ is larger.

CONCLUSION

A numerical model, which is based on Simplified Marker and Cell(SMAC) method and Monotone Upstream-centered Schemes for Conservation Laws (MUSCL) technique, is constructed to simulate two-dimensional density surges, initiated by a finite volume release of dense fluid into a finite ambient water depth on a horizontal bed. The density difference is due to either salinity or mixture of nearly uniform sized particles and water. Comparisons with experimental results of maximum height, propagation speed, mean effective gravity force and densimetric Froude number at the front of the surge show that the present model simulates wellthe motion of the conservative density surges. The following relationships were found to exist: $U/(W_0^2/A_0)^{1/4}$, $H/\sqrt{A_0}$, $B/(W_0/A_0)$, and Fr are almost constant with $x_f/\sqrt{A_0}$ in the slumping regime: on the other hand, $U/(W_0^2/A_0)^{1/4} \sim (x_f/\sqrt{A_0})^{-1/2}$, $B/(W_0/A_0) \sim (x_f/\sqrt{A_0})^{-1}$, while both H and Fr are almost constant with $(x_f/\sqrt{A_0})^{-1/2}$ in the inertia-buoyancy regime. It is also found from numerical experiments for conservative density surges that the transition point from the slumping regime to the inertia-buoyancy regime is controlled by the parameter $h/\sqrt{A_0}$.

ACKNOWLEDGMENT

This study was supported by the Grant in Aid for Scientific Research of the Ministry of Education and Culture, Japan, under Grant B(2)12555149.

REFERENCES

1. Akiyama, J., M., U., Tomioka, N. and Suehiro, Y.: Flow characteristics of thermals on low slope angles, *Annual Journal of Hydraulic Engineering*, Vol. 42, pp. 511–516, 1998, (in Japanese).
2. Akiyama, J. and Ura, M.: Motion of 2D buoyant clouds downslope, *Journal of Hydraulic Engineering,* ASCE, Vol. 125, No. 5, pp. 474–480, 1999.
3. Akiyama, J., Ura, M. and Wang, W.: Physical-based numerical model of inclined starting plumes, *Journal of Hydraulic Engineering,* ASCE, Vol. 120 (10), pp. 1139–1158, 1995.
4. Akiyama, J., Ying, X., Ura, M. and Shigeeda, M.: Numerical simulation for dumped fine particles in quiescent water with finite depth, *Journal of Hydraulic, Coastal and Environmental Engineering*, No. 663/II-53, pp. 43–53, 2000, (in Japanese).
5. Amsden, A. A. and Harlow, F. H.: A simplified MAC technique for incompressible fluid flow calculations, *Journal of Computational Physics*, Vol. 6, pp. 322–325, 1970.
6. Beghin, P., Hopfinger, E. J. and Britter, R. E.: Gravitational convection from instantaneous sources on inclined boundaries, *Journal of Fluid Mechanics*, Vol. 107, pp. 407–422, 1981.
7. Benjamin, T. B.: Gravity currents and related phenomena, *Journal of Fluid Mechanics*, Vol. 31, pp. 209–248, 1968.
8. Bonnecaze, R. T., Huppert, H. E. and Lister, J. R.: Particle-driven gravity currents, *Journal of Fluid Mechanics*, Vol. 250, pp. 339–369, 1993.
9. Britter, R. E. and Linden, P. F.: The motion of the front of a gravity current traveling down an incline, *Journal of Fluid Mechanics*, Vol. 99, pp. 531–543, 1980.
10. Cheong, H.-B. and Han, ho Y.: Numerical study of two-dimensional gravity currents on a slope, *Journal of Oceanograph*, Vol. 53, pp. 179–192, 1997.

11. Eto, T. and Fukushima, Y.: Numerical analysis of conservative inclined thermals using $k-\epsilon$ turbulence model, *Annual Journal of Hydraulic Engineering*, Vol. 46, pp. 1043–1048, 2002, (in Japanese).

12. Hopfinger, E. J.: Snow avalanche motion and related phenomena, *Annual Review of Fluid Mechanics*, Vol. 15, pp. 47–76, 1983.

13. Hopfinger, E. J. and Tochon-Danguy, J. C.: A Model study of powder-snow avalanches, *Journal of Glaciology*, Vol. 19, pp. 343–356, 1977.

14. Hosoda, T., Nishizawa, K., Fukusumi, A., Okubo, K. and Muramoto, Y.: Numerical studies on internal waves induced in a densimetric exchange flow, *Annual Journal of Hydraulic Engineering*, Vol. 40, pp. 525–530, 1996, (in Japanese).

15. Hoult, D. P.: Oil spreading on the sea, *Annual Review of Fluid Mechanics*, Vol. 4, pp. 341–368, 1972.

16. Huppert, H. E. and Simpson, J. E.: The slumping of gravity currents, *Journal of Fluid Mechanics*, Vol. 99, part4, pp. 785–799, 1980.

17. Jha, A. K., Akiyama, J. and Ura, M.: Simulation of gravity currents by flux-difference splitting scheme, *Annual Journal of Hydraulic Engineering,* JSCE, Vol. 46, pp. 1037–1042, 2002.

18. Morton, B. R., Taylor, G. I. and Turner, J. S.: Turbulent gravitational convection from maintained and instantaneous sources, *Proceedings of Royal Society of London,* A234, pp. 1–23, 1983.

19. Nakayama, K. and Satoh, T.: Analysis of plumes on horizontal surface by LES model, *Journal of Hydraulic, Coastal and Environmental Engineering*, No. 628/II-48, pp. 97–114, 1998, (in Japanese).

20. Rottman, J. W. and Simpson, J. E.: Gravity currents produced by instantaneous release of a heavy fluid in a rectangular channel, *Journal of Fluid Mechanics*, Vol. 135, pp. 95–110, 1983.

21. Rubey, W. N.: Settling velocities of gravel, sand and silt particles, *Amer. Jour. Sci.*, Vol. 25, pp. 325–338, 1933.

22. Simpson, J. E.: Gravity currents in the laboratory, atmosphere, and ocean, *Annual Review of Fluid Mechanics*, Vol. 14, pp. 213–234, 1982.

23. Simpson, J. E. and Britter, R. E.: The dynamics of the head of agravity current advancing over a horizontal surface, *Journal of Fluid Mechanics*, Vol. 94, pp. 477–495, 1979.

24. Leer, van B.: Toward the ultimate conservative difference scheme. 4 A new approach to numerical convection, *Journal of Computational Physics*, Vol. 23, pp. 276–299, 1977.

25. Yih, C. S.: *Stratified Flows*, Academic Press, 1980.

26. Ying, X., Akiyama, J. and Ura, M.: Numerical study of 2-D inclined starting plumes using LES, *Journal of Hydroscience and Hydraulic Engineering*, Vol. 17, No. 1, pp. 117–129, 1999.

APPENDIX-NOTATION

The following symbols are used in this paper:

A = area of the front of the surge;

A_0 = inital fixed volume of dense water;

B = mean effective gravity force of the front of the surge;

c = volumetric concentration;

d = median diameter of partilce;

D_m = diffusivity ($=\nu/S_{ct}$);

Fr = densimetric Froude number ($=U/\sqrt{\epsilon g H}$);

g = acceleration due to gravity;

H = maximum height of the front of the surge;

n = index for time;

S_{ct} = Schmidt number;

t = time;

U = propagation speed of the front of the surge;

u, v = flow velocities along x- and y- direction, respectively;

V_s = settling velocity of a particle;

p = pressure;

s = submerged specific gravity of particle;

W = effective gravity force;

W_0 = total initial effective gravity force;

x_f = location of front of the surge;

ϵ = relative density difference;

ρ = density of solid-liquid mixture;

ρ_a = density of ambient fluid;

ν = kinematic viscosity of fluid;

ϕ = scalar potential corresponding to time change of pressure;

Δx, Δy = grid size in x, y direction; and

σ = specific gravity of particle.

(Received September 10, 2003 ; revised November 19, 2003)